

Article

Surface Polishing of an Inconel 625 Bar by a Super-Fast MAF Process for a Solenoid Valve Stem Used in a Hydrogen Tank

Hwi-Joong Kim ^{1,*}, Lida Heng ^{1,*}  and Sang-Don Mun ^{1,2,*}

¹ Department of Mechanical Design Engineering, Jeonbuk National University, Jeonju 54896, Republic of Korea; joong5123@jbnu.ac.kr

² Department of Energy Storage/Conversion Engineering of Graduate School, Jeonbuk National University, Jeonju 54896, Republic of Korea

* Correspondence: henglida1@gmail.com (L.H.); msd@jbnu.ac.kr (S.-D.M.); Tel.: +82-63-270-4762 (S.-D.M.)

Abstract: This study explores a super-fast magnetic abrasive finishing (MAF) process for polishing the surface of an Inconel 625 bar workpiece for a hydrogen solenoid valve stem. The Inconel 625 bar was chosen to replace the existing STS 316 bar material, previously used for a hydrogen solenoid valve stem. The cylindrical surface of Inconel 625 bars was polished by a super-fast MAF process with high rotational speeds of 1000, 5000, 15,000, and 25,000 RPM and a super-strong magnetic field of 550 mT. The polishing characteristics of this process were evaluated according to the type of abrasives, rotational speeds of the workpiece and processing time. As a result, a super-smooth Inconel 625 bar was successfully achieved, with a surface roughness (Ra) reduced from 0.31 μm to 0.02 μm under the optimal conditions (15,000 RPM, CNT particles (0.04 μm), PCD diamond abrasive (1 μm), Fe (#200), 0.5 g of light oil, and 16 min of processing time). Also, the Ansys analysis results showed suitable strain, equivalent stress, and safety factor of the Inconel 625 bar. This confirmed that, after a super-fast MAF process, an Inconel 625 bar is feasible for application in Hydrogen (H₂) tanks instead of a conventional STS 316 bar.

Keywords: super-fast magnetic abrasive finishing (MAF) process; hydrogen solenoid valve stem; surface roughness; Inconel 625 bar; equivalent stress



Citation: Kim, H.-J.; Heng, L.; Mun, S.-D. Surface Polishing of an Inconel 625 Bar by a Super-Fast MAF Process for a Solenoid Valve Stem Used in a Hydrogen Tank. *Metals* **2024**, *14*, 242. <https://doi.org/10.3390/met14020242>

Academic Editor: John Campbell

Received: 26 November 2023

Revised: 13 February 2024

Accepted: 13 February 2024

Published: 16 February 2024



Copyright: © 2024 by the authors. Licensee MDPI, Basel, Switzerland. This article is an open access article distributed under the terms and conditions of the Creative Commons Attribution (CC BY) license (<https://creativecommons.org/licenses/by/4.0/>).

1. Introduction

Hydrogen solenoid valves are electrically controlled valves that are widely used to control the ON/OFF flow of hydrogen in a hydrogen tank [1–3]. They are mostly composed of a valve body, a solenoid coil, a locking nut, a valve housing, a spring, a plunger, an orifice, and a needle valve (also called solenoid valve stem) [4]. The solenoid valve stem or needle valve plays an important role in high-pressure hydrogen flow in solenoid valves [5,6]. It directly affects the flow characteristics of hydrogen in the valve and contributes to the working performance and safety of the high-pressure hydrogen valve [7,8]. Currently, the cylindrical STS 316 bar is widely used as a solenoid valve (STEM) in hydrogen tanks. It is commonly utilized for opening and closing of the hydrogen flow in the pipeline of hydrogen tanks. STS 316 bars are austenitic stainless-steel materials with high corrosion resistance but relative vulnerability to hydrogen embrittlement, particularly in high-pressure environments. Matsuoka and Takaki et al. [3,9] reported that austenitic stainless steel is the most common hydrogen-resistant material that is currently used for hydrogen flow applications. However, high ambient temperatures and stress are commonplace in high-pressure hydrogen facilities. It is clear that austenitic stainless steel cannot match the strength needs of high-pressure hydrogen (H₂) environments [10].

Therefore, a superior material such as Inconel 625 bars is needed to solve the limitations of STS 316 bars used in a high-pressure hydrogen system. Inconel 625 is a Ni–Cr high-strength alloy with excellent resistance to limit hydrogen absorption and shows high

heat resistance in high-temperature and high-pressure environments as well as high corrosion resistance in low-temperature and high-pressure environments. According to Hicks et al. [11,12], the Inconel 625 alloy had a higher resistance to hydrogen compared with Inconel 718 and iron-based nickel chrome austenitic stainless (A286) alloy. Thus, Inconel 625 alloy can be used in situations with high hydrogen pressure.

All types of valves used for needle-shaped STEM parts are very closely related to the surface roughness of STEM because they are directly contacted by high-pressure hydrogen. In other words, it is important to secure high surface roughness in the initial production stage because an inferior surface roughness is more likely to allow leakage of target substances such as hydrogen, and it is possible for energy to accumulate during long-term leakage, leading to fatigue destruction. Therefore, a super-smooth surface with low roughness is needed for the solenoid valve stem for application in a high-pressure hydrogen system. In general, there are many methods that can be used to improve or achieve a smooth surface of materials with different shapes such as circular pipes [13], cylindrical bars [14], flat [15,16], and grooved [17,18].

In previous works, Singh et al. [19] applied the magnetorheological (MR) finishing process for polishing the cylindrical surface of a workpiece made of AISI grade D2 tool steel using SiC abrasive particles. His results showed that the average surface roughness (Ra) value of the workpiece was reduced from 0.7 μm to 0.019 μm within 120 min of the processing time. Singh et al. [20] also applied this process to the ultra-polishing surface of a cylindrical bar roller made of copper by Al_2O_3 abrasive particles. He found that the surface roughness of the workpiece was reduced from 0.19 μm to 0.025 μm after 240 min of the polishing time. Rana et al. [21] used the MR finishing process for fine finishing of the stepped cylindrical workpiece bar made of aluminum (Al) alloy using magnetic abrasive tools (a mixture of iron particles and alumina abrasive particles). After 40 min of the polishing time, the surface roughness (Ra) value was reduced from the initial surface roughness of 0.284 μm to 0.062 μm . Nguyen et al. [22] applied the lapping and polishing process for improving the surface quality of cylindrical bar roller bearing in made of GCr15 alloy. He found that surface roughness (Ra) value of workpiece could be decreased from 0.5 μm to 0.063 μm after 180 min of the lapping process, and decreased to 0.013 μm after 60 min of the polishing process.

The above review of the previous papers revealed that besides the magnetic abrasive finishing process, there are few processes (e.g., magnetorheological (MR) finishing, lapping, and polishing process) that could be used to reduce the surface roughness value of cylindrical bar workpieces resulting in achieved their smooth surface. However, they all require a large processing time, which is a major limitation. Moreover, it is very difficult to achieve a super-smooth surface of cylindrical bars using the current methods within a short processing time. When a workpiece to be finished is a cylindrical Inconel 625 bar, the use of current processes is very difficult due to the characteristic alloy of the cylindrical Inconel 625 bar. Inconel 625 is a nickel-based alloy that is difficult to cut because of its low thermal conductivity, high hardness, high strength, and low elastic modulus [23,24]. Moreover, some of the current polishing techniques use high-pressure polishing tools with low control, which can cause micro-cracks on the surface of a cylindrical Inconel 625 bar.

To overcome these limitations, a super-fast magnetic abrasive finishing (MAF) process is used with a super-strong magnetic field to polish the cylindrical surface of an Inconel 625 bar used for a hydrogen solenoid valve stem. This fabrication process applies a high rotational speed (1000, 5000, 15,000, and 25,000 RPM) and a super-strong magnetic field (550 mT) to reduce the surface roughness of a cylindrical Inconel 625 bar, resulting in a super-smooth surface polish. The polishing tool used in this study is a mixture of magnetic abrasives (Fe powder, CNT mixed with diamond paste, and lubricant). This mixture is applied to a flexible magnetic abrasive brush that is controlled by a super-strong magnetic field to remove roughness from the surface of a cylindrical Inconel 625 bar.

The aim of this study is to achieve a super-smooth surface of cylindrical Inconel 625 bars to be used for a solenoid valve stem in a hydrogen tank. The cylindrical surface of

Inconel 625 bars were polished by a super-fast magnetic abrasive finishing (MAF) process. The polishing characteristics of this process were investigated and evaluated under polishing parameters of rotational speed, type of abrasive tools, and polishing time. Finally, Ansys workbench finite element analysis was used to evaluate the strain, equivalent stress, and safety factor of the Inconel 625 bars and to compare the results with those of the STS 316 currently used for the solenoid valve stem.

2. Material Selection

Inconel alloys are a unique product of the Special Metals Corporation (New Hartford, NY, USA), manufactured as a combination of carbon, iron, chromium, and nickel. They are widely used in a variety of advanced industries due to their superior mechanical and physical properties such as high heat resistance, corrosion resistance, and oxidation resistance and can maintain high strength at high-temperature environments [25]. Based on nickel, Inconel is divided into 600, 625, 718, and X750 depending on the content of elements such as iron, chromium, niobium, and molybdenum [26]. In this study, non-magnetic Inconel 625 bars were used as the workpiece, which was produced by GPLEX Corporation Co., Ltd., Uiwang-si, Gyeonggi-do, Republic of Korea, and they had a diameter of $\varnothing 6$ mm with the original surface roughness R_a values of $0.31 \mu\text{m}$. To fabricate the needle valve (solenoid valve stem), the Inconel 625 bars were initially cut into 100 mm long round bars by the lathe machine (model: Hwacheon (HL-380–750)) (Gwangsan-gu, Gwangju, Republic of Korea) with a rotational speed of 335 RPM. Also, their single-sided edge was machined into a 45° cone shape at one end to match the stem of the needle opening and closing valve. A detailed dimensional view and a photograph of non-magnetic Inconel 625 bars are shown in Figure 1 and Figure 2, respectively. The chemical composition and mechanical properties of the workpiece used in the experiment are listed in Table 1 and Table 2, respectively.

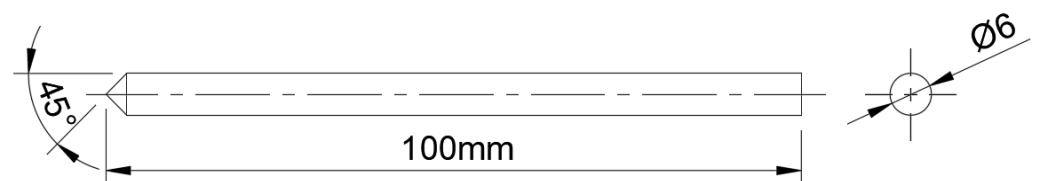


Figure 1. Dimensional view of the Inconel 625 alloy bars.

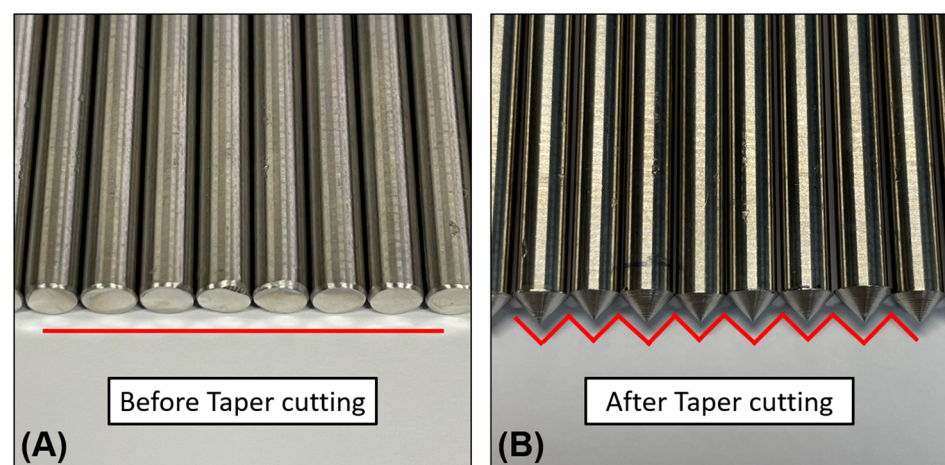


Figure 2. (A) Photographs before machining of Inconel alloy workpiece and (B) after machining.

Table 1. Chemical composition of the Inconel 625 alloy % mass.

Al	Cr	Fe	Mo	Nb	Ti	Ni
0.16	21.5	4.6	8.7	3.32	0.18	Base

Table 2. Mechanical properties of Inconel 625 alloy.

Young's Modulus (MPa)	Yield Strength (MPa)	Density (kg/m ³)	Poisson's Ratio
2.1×10^5	516	7.8×10^{-9}	0.28

3. Experimental Setup and Polishing Principle of the Super-Fast MAF Process

The magnetic abrasive finishing (MAF) process is an advanced mechanical polishing method to produce a very smooth surface of materials or products by reducing their surface roughness. This process is unlike the traditional processing methods that apply high-pressure cutting or polishing on the surface of materials. Instead, the MAF process uses low cutting force with flexible abrasive tools treated with a strong flux density of a permanent magnet to remove the protruding material from a surface.

However, the MAF process has a major limitation—the difficulty of polishing the surface of materials such as Inconel 625 or ceramics [27,28]. Unlike the current MAF process that uses a permanent magnet [29] or electromagnet [30] as the magnetic field generator, the super-fast MAF process used in this study is a novel hybrid magnetic polishing technique. This technique combines a neodymium permanent magnet (Nd-Fe-B) and electromagnets for more efficient polishing of a hard material such as Inconel 625. Figure 3 shows a schematic diagram of the super-fast MAF system of a super-fast air spindle with hybrid magnets for polishing an Inconel 625 bar. As shown in Figure 3, the polishing system can be divided into a super-fast rotational workpiece, which can rotate up to 125,000 rpm, and a hybrid magnet of permanent and electromagnetic parts. To rotate the Inconel 625 workpiece, a super-fast air spindle uses a compressed air system with a rotational speed controller that can adjust the speed in the range of 1000–125,000 RPM. This spindle is fixed with bolts to an aluminum support so that it is not affected by fine vibrations generated during processing, and four pneumatic tube fittings are installed at the bottom, for compressed air injection and exhaust and for cooling water injection and discharge. The workpiece stimulation part concentrates the magnetic field generated by the neodymium (Nd-Fe-B) permanent magnet to ensure that the magnetic tool remains attached to the workpiece that rotates at high speed during processing. In addition, the stimulation part generates a stronger physical force through magnetic concentration to increase the compressive force of the magnetic tool and the workpiece. A hybrid of permanent and electromagnets was used to generate the strong magnetic field. Typical characteristics of an electromagnet are the adjustable strength of the magnetic field and its generation only when desired. However, electromagnets have a complex, bulky structure involving a control system and a power supply. While a permanent magnet does not require an external energy supply and has a simple structure, the strength of its field decreases over time, and it is difficult to change the amplitude and direction of the magnetic field. Therefore, these two types of magnets are combined to allow adjustment of the flux density of the magnetic field to 550 mT. A 550 mT magnetic field is strong enough to control the magnetic abrasive tools used to polish the surface of Inconel 625.

Figure 4 shows the polishing principle of the super-fast MAF process with an Inconel 625 bar in a hydrogen tank. Figure 4a is a photograph of the polishing machine, while Figure 4b shows its schematic view. In this process, the Inconel 625 bar is placed in the gap between the poles (N pole-S pole) of Nd-Fe-B magnets and connected to the super-fast air spindle. A spindle speed in the range of 1000–125,000 RPM allows contact with the magnetic abrasive (mixture of Fe powder, abrasive tools, and light oil) attached to the edges of the magnetic poles. The relative motion between the magnetic abrasive and the surface of the bar removes the roughness to produce a very smooth surface of the Inconel 625 bar.

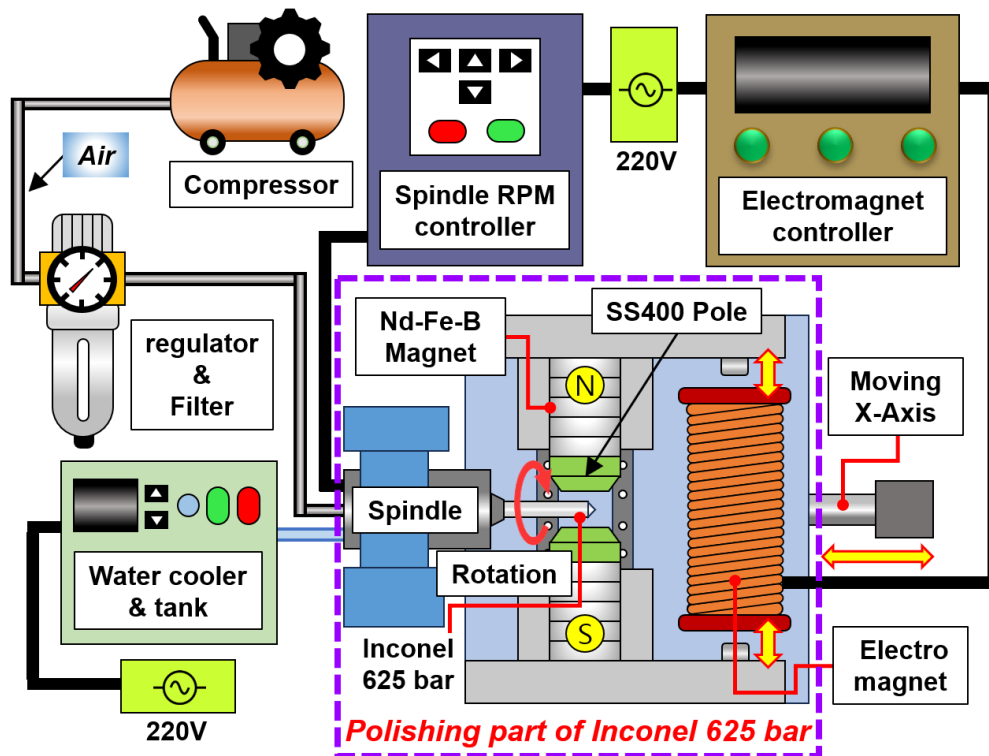


Figure 3. Schematic diagram of a super-fast MAF machine using a super-fast air spindle with hybrid magnets for polishing an Inconel 625 bar.

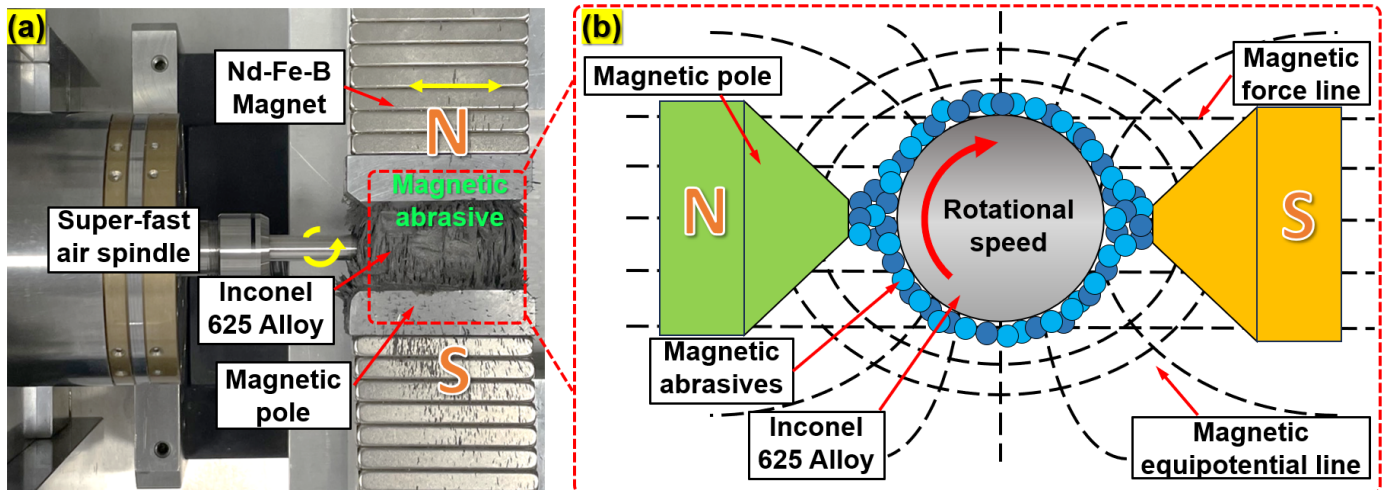


Figure 4. Polishing principle of the super-fast MAF process for an Inconel 625 bar used for a hydrogen (H_2) tank: (a) Photographic view and (b) schematic view.

4. Experimental Method and Conditions

4.1. Experimental Conditions

The optimal processing conditions were assessed by varying the rotational speeds of the Inconel 625 bar workpieces, the type of abrasive materials, and the temperature of the processing part at fixed conditions of polishing liquid, stimulation shape, and magnetic flux density. The rotational speed was set in order as 1000, 5000, 15,000, and 25,000 RPM. The processing time was set as 0, 4, 8, 12, and 16 min. There were three kinds of abrasive used in this study—a combination of CNT with diamond paste (1st), Al_2O_3 (2nd), and SiC (3rd). More detailed experimental conditions are shown in Table 3.

Table 3. Experimental conditions.

Parameter	Value
Workpiece	Inconel 625 bar (dimension: $\varnothing 6 \times 100$ mm)
Rotational speed (RPM)	1000, 5000, 15,000, 25,000
Magnetic abrasive (g)	Fe powder: 9.0 g (#200) (i) CNT: 0.05 g (0.04 μm) + diamond paste: 1 g (1 μm) (ii) Al_2O_3 : 0.7 g (0.05 μm) (iii) SiC: 2.0 g (#320)
Lubricant (g)	Light oil: 0.5 g
Processing time (min)	0, 4, 8, 12, 16
Pole shape	Trapezoid
Pole material	SS400 steel
Amplitude (mm)	1
Magnet size (mm)	$30 \times 20 \times 10$
Magnetic flux density (mT)	550

4.1.1. MAF Tools

In this study, a mixture of electrolytic iron (Fe) powder, abrasive particles, and lubricant was used as the polishing tools. The abrasive particles used in this experiment were a CNT with diamond compound, Al_2O_3 , and SiC, which were used directly to polish the surface of the Inconel 625 bar. Figure 5 shows images of a mixture of magnetic abrasive tools. Figure 5a is Fe powder; Figure 5b is a combination of CNT with diamond paste (1st), Al_2O_3 (2nd), and SiC (3rd); Figure 5c is lubricant; and Figure 5d is the product mixture MAF tools. As shown in Figure 5, 1 g, 0.05 g, 0.7 g, and 2 g of the remaining polishing particles were used with 9 g of electrolytic iron and 0.05 mL of polishing solution.



Figure 5. Images of a mixture of magnetic abrasive tools: (a) Fe powder; (b) CNT + diamond paste (1st), Al_2O_3 (2nd), and SiC (3rd); (c) lubricant, and (d) their mixture to produce an MAF tool.

The diamond compound used in this experiment was of the polycrystalline diamond (PCD) abrasive type (Allied High-Tech Products, Inc., Compton, CA, USA), while the carbon nanotube (CNT), aluminum oxide (Al_2O_3), and silicon carbide (SiC) abrasives were obtained from Jung Do Tech Co., Ltd., Jeollabuk-do, Republic of Korea. The electrolytic iron particles used in this experiment helped to produce adhesion to the surface of the workpiece due to the nature of the ferromagnetic body and prevented the abrasive from spreading beyond the magnetic range at high rotational speed. High-purity iron powder (Fe) was

obtained from Jung Do Tech Co., Ltd., Jeollabuk-do, Republic of Korea. The lubricant used in this experiment was light oil from WD-40 Company Ltd., Jeollabuk-do, Republic of Korea. It reduces frictional heat generated during the polishing process and agglomerates the abrasion debris to prevent loss of performance of the abrasive. The CNT abrasives used in this experiment were multiwalled nanotube (MWNT) particles, which were used as additional abrasives with the aim of producing a fine surface of cylindrical Inconel 625 bar. These abrasives have the advantages such as light weight and very small grain size with a high strength cutting edge that can produce a fine surface of the workpiece when they are mixed with the mixture of the diamond abrasive and electrolytic iron particles. The mechanical properties of each type of abrasive particle used in this experiment are shown in Table 4. Diamonds are classified as natural abrasives, and SiC and Al₂O₃ (alumina) are classified as artificial abrasives and are ceramic materials. All four types of abrasives have very high strength, though the CNT abrasive and diamond abrasive particles have the advantage of being significantly higher strength than alumina oxide and silicon carbide.

Table 4. Abrasive particle properties used in the experiment (adapted from [31–34]).

Mechanical Properties	CNT Abrasive Particles	Diamond Abrasive in Paste	Alumina Oxide (Al ₂ O ₃)	Silicon Carbide (SiC)
Density (Mg/m ³)	1.6	3.44	3	4.36
Thermal conductivity (W/mK)	1800~6600	350	30	70~110
Strength (GPa)	20~50	4.0	1.5	2.9
Young's modulus (GPa)	1200	1050	215–413	90
Tensile strength (MPa)	150,000	2800	69	240
Elastic modulus (GPa)	600~1200	1050	380	210

4.1.2. Measurements

In order to evaluate the main surface roughness improvement after polishing by the super-fast MAF process, the surface roughness values Ra of Inconel 625 bars were measured before and after the polishing process.

The surface roughness measurement equipment (model: SJ-400 Mitutoyo) (Mitutoyo, Sakado, Japan) was a contact type that detects changes as if drawing along the surface using a tentacle among contact and contactless measuring instruments and calculates measurement results based on roughness curves. Figure 6 shows the images of the surface roughness measurement equipment and the method for measuring the surface of Inconel 625 bars. Figure 6a shows a full image of the surface roughness measuring process by SJ-400 Mitutoyo equipment for the Inconel 625 bar workpiece. Figure 6b shows an enlarged view of the measuring process on the surface of the workpiece. Figure 6c shows the measuring method at three different points on the surface of the workpiece. In this study, the total processing time of the super-fast MAF process was 16 min and a total of five surface roughness measurements were performed in 4 min increments to measure and compare the surface condition before and after processing.

In order to calculate the average surface roughness (Ra) value improvement before and after the magnetic abrasive finishing process, three points on the surface area of the workpiece were measured (see Figure 6c), and their average values were recorded in micrometers as below:

$$\bar{R}_a = \frac{1}{n} \sum_{i=1}^n R_{a_i} \quad (1)$$

where \bar{R}_a is an average surface roughness value (μm), n is the number of values, R_{a_i} is a date value of the roughness of each measurement point (μm).

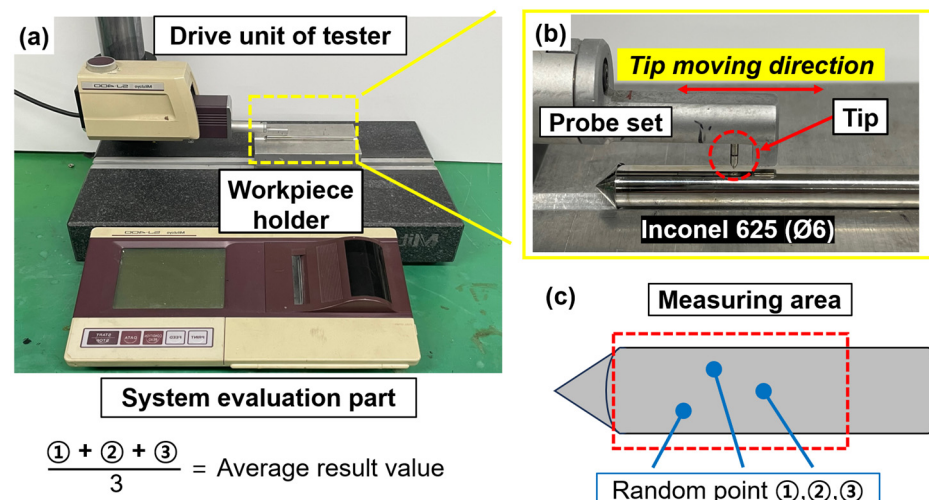


Figure 6. (a) Surface roughness measuring equipment, (b) an enlarged view of the measuring process, and (c) measuring method at three different points on the surface of the workpiece.

5. Results and Discussion

5.1. Surface Roughness with Rotational Speed

Figure 7 shows the surface roughness improvement of Inconel 625 bars at different rotational speeds (1000, 5000, 15,000, and 25,000 RPM) using the magnetic abrasive tools (i) CNT + diamond paste. Figure 8 illustrates the schematics of the rotational motion of the Inconel 625 bar during the super-fast MAF process at different rotational speeds. Figures 9 and 10 show the surface roughness improvement of Inconel 625 bars at different rotational speeds (1000, 5000, 15,000, and 25,000 RPM) using the different types of magnetic abrasive tools: (ii) Al_2O_3 , and (iii) SiC abrasives. Figure 7 shows the change in surface roughness R_a when using the CNT mixed with diamond paste. For CNT mixed with diamond paste, the R_a value of the Inconel 625 bar decreased from $0.31 \mu\text{m}$ to $0.11 \mu\text{m}$ after 4 min of processing at 1000 rpm, to $0.05 \mu\text{m}$ after 8 min, to $0.04 \mu\text{m}$ after 12 min, and to $0.03 \mu\text{m}$ after 16 min of processing. At 5000 rpm, the R_a value decreased rapidly from $0.31 \mu\text{m}$ to $0.04 \mu\text{m}$ after 4 min of processing and remained at that value after 8 min and 12 min. Finally, after 16 min of processing, the R_a value of the bar was $0.03 \mu\text{m}$. At 15,000 rpm, the R_a was reduced from $0.31 \mu\text{m}$ to $0.06 \mu\text{m}$ after 4 min, to $0.05 \mu\text{m}$ after 8 min, $0.05 \mu\text{m}$ after 12 min, and finally showed the best R_a of $0.02 \mu\text{m}$ after 16 min. At 25,000 rpm, the R_a of the bar was decreased from $0.31 \mu\text{m}$ to $0.04 \mu\text{m}$ after 4 min, increased to $0.07 \mu\text{m}$ after 8 min, improved to $0.03 \mu\text{m}$ after 12 min, and finally was $0.03 \mu\text{m}$ after 16 min. The surface roughness R_a values of Inconel 625 bars were reduced at all rotational speeds (e.g., 1000, 5000, 15,000, and 25,000 RPM) by super-fast MAF process using CNT + diamond paste. Among the four rotational speeds, 15,000 rpm produced the best result, $0.02 \mu\text{m}$. This is accounted for by the fact that when the rotational speed of the Inconel 625 bar increased to 15,000 rpm, a greater enhancement in surface roughness value was achieved. Equation (2) provides an explanation for this. In this polishing process, a smooth surface of the Inconel 625 workpiece is achieved by the polishing speed (V_p) of abrasive particles on the surface of the workpiece. This speed is related to the rotational speed of the workpiece. The rate of polishing is directly linked to the rotational speed (RPM) of the workpiece. As per Equation (2), elevating the RPM of an Inconel 625 bar workpiece results in an increase in the polishing speed (V_p) of the abrasive particles on the surface of the Inconel 625 bar also increases. This allows for faster removal of rough sections from the surface of the workpiece.

However, there was a rising run-out of the workpiece when the Inconel 625 workpiece's rotational speed was increased to 25,000 RPM. As the run-out increased, the R_a value of the workpiece at the polishing area increased. This is due to the harsh collision between abrasive particles and the surface of the workpiece during the polishing process.

Figure 8a illustrates a normal rotational speed of the Inconel 625 bar when it was rotated normally (no run-out) at 15,000 RPM on the top and front view. Figure 8b illustrates a run-out of the Inconel 625 bar that occurred at the exceeding rotational speed of 25,000 RPM. The run-out of the Inconel 625 bar leads it to inaccurate rotation or spinning off the rotation center (see Figure 8b). Thus, the frictional force and collision rate between the surface of the Inconel 625 bar and abrasive particles increased, resulting in worse surface polishing when compared to 15,000 RPM of rotational speed.

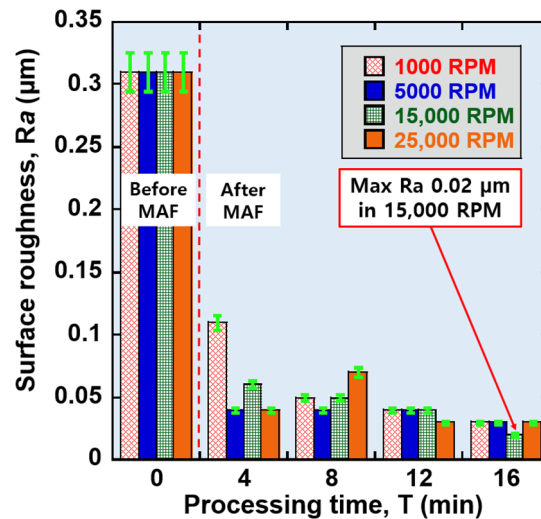


Figure 7. Graph of changes in surface roughness Ra value of Inconel 625 bars when CNT + diamond paste was used as the abrasive particle.

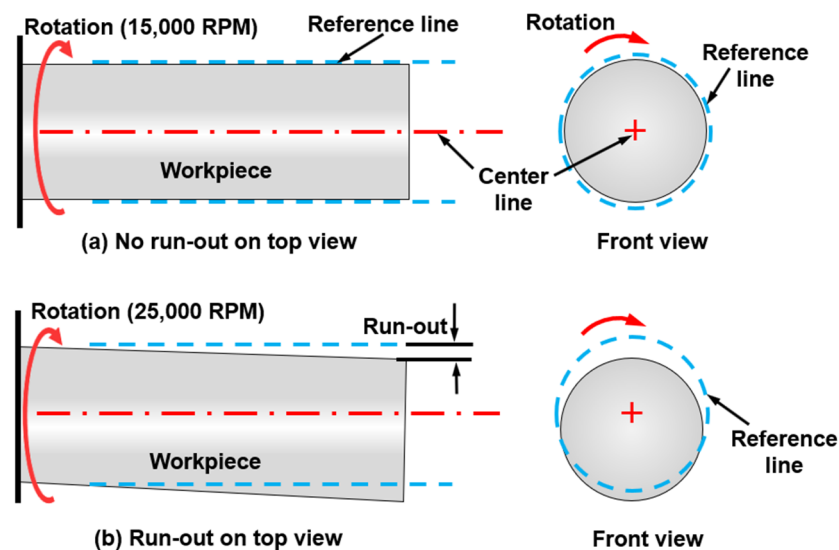


Figure 8. Schematics of rotational motion of the Inconel 625 bar during the super-fast MAF process: (a) no run-out at 15,000 RPM, and (b) run-out at 25,000 RPM.

Figure 9 shows the change in surface roughness Ra when using alumina (Al_2O_3) as the abrasive. The surface roughness decreased at all rotational speeds by the super-fast magnetic abrasive finishing (MAF) process using alumina abrasive. The results showed that the Ra value of the Inconel 625 bar decreased from $0.31 \mu\text{m}$ to $0.11 \mu\text{m}$, $0.08 \mu\text{m}$, $0.03 \mu\text{m}$, and $0.06 \mu\text{m}$ at rotational speeds of 1000 rpm, 5000 rpm, 15,000 rpm, and 25,000 rpm, respectively, after 16 min of the processing time. At 15,000 rpm, the best Ra value of the Inconel 625 bar was achieved at $0.03 \mu\text{m}$. Figure 10 shows the change in the Ra value of Inconel 625 bars when using SiC abrasive particles. The Ra value of Inconel 625 bars was reduced at all speeds by super-fast MAF using SiC abrasive. The Ra of $0.31 \mu\text{m}$ was

reduced to 0.15 μm , 0.11 μm , 0.06 μm , and 0.13 μm after polishing for 16 min at rotational speeds of 1000 rpm, 5000 rpm, 15,000 rpm, and 25,000 rpm, respectively. However, the surface roughness Ra values of Inconel 625 bars were difficult to reduce to 0.06 μm when the SiC abrasive was used.

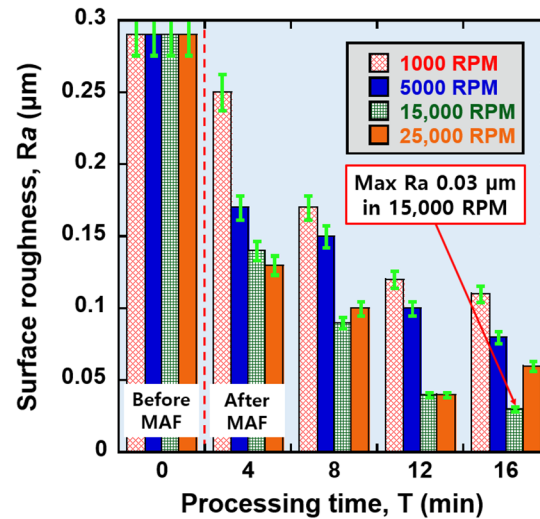


Figure 9. Graph of changes in surface roughness Ra value of Inconel 625 bars when Al_2O_3 was used as the abrasive particle.

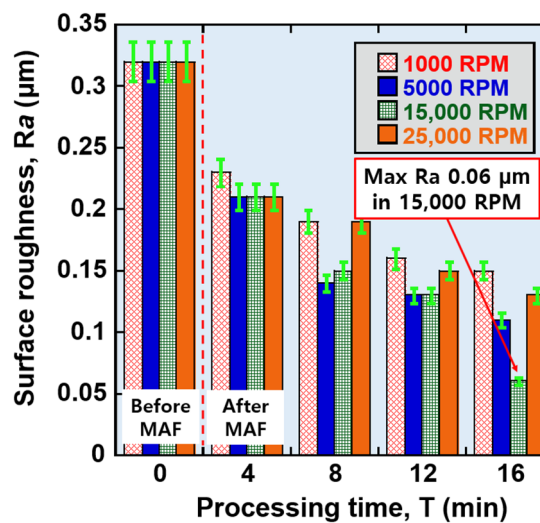


Figure 10. Graph of changes in surface roughness Ra value of Inconel 625 bars when SiC was used as the abrasive particle.

By comparing the reduction in Ra value results, we find that the Ra values of the Inconel 625 bar were reduced to 0.02 μm , 0.03 μm , and 0.06 μm by the CNT + diamond paste, Al_2O_3 , and SiC abrasives, respectively. According to Table 4, the mechanical properties of CNT + diamond paste (such as strength, and elastic modulus) are significantly greater than the other abrasives. Due to this reason, CNT + diamond paste can effectively remove the rough parts (i.e., scratches and unevenness) from the surface of Inconel 625 bars when compared to the other abrasives.

$$V_p = \frac{\pi \times D \times \text{RPM}}{1000} \quad (2)$$

where V_p is the polishing speed of abrasive particles (mm/s), RPM is the rotational speed of the Inconel 625 bar (revolutions/min), D is the diameter of the Inconel 625 bar (mm), and π is a circular constant.

5.2. Surface Observation

Figure 11 shows photographs and $500\times$ SEM micro images comparing the surface of the Inconel 625 bar before and after the super-fast MAF process. Figure 11a is an image of the original workpiece before treatment, with an Ra value of $0.31\ \mu\text{m}$ and a very rough surface with poor qualities such as blurriness and low reflection. Figure 11b is an image after polishing for 16 min at 15,000 rpm using a CNT + diamond abrasive. The best surface roughness reduction was obtained at these conditions, producing an Ra value of $0.02\ \mu\text{m}$. Figure 11b shows the high surface quality with a mirror-like surface producing high reflection. Figure 11c,d shows a $500\times$ SEM micro image of the surface before and after processing. The initial surface was rough, with multiple grooves of different depths (see Figure 11c). Figure 11d shows the surface after processing, with the removal of all rough structures. The results confirm that the super-fast MAF process can reduce material surface roughness to produce a super-smooth surface on materials.

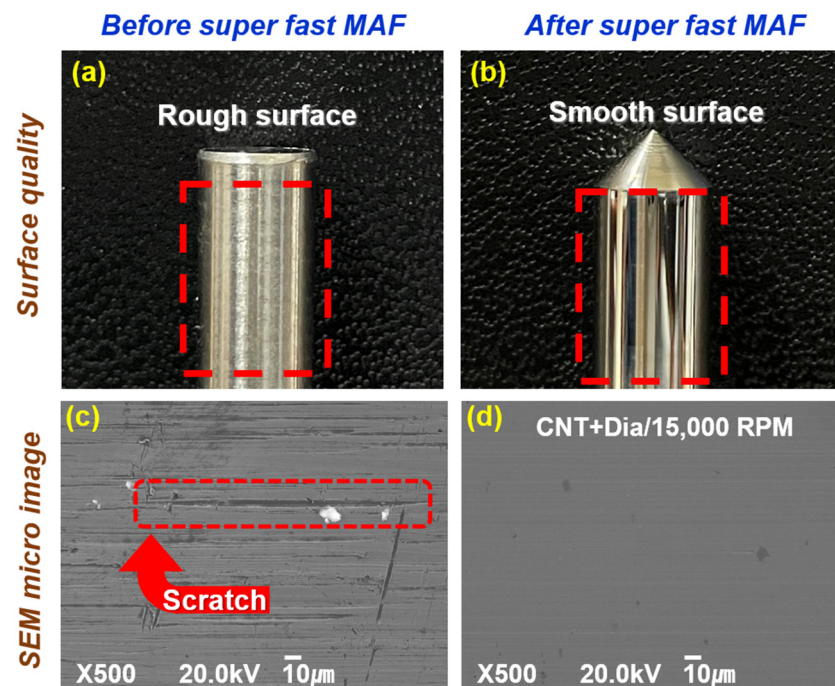


Figure 11. Photographs and SEM micro images comparing the surface of the Inconel 625 bar before and after the super-fast MAF process: (a) an image of the original workpiece before treatment, (b) after treatment, (c) SEM micro images of original workpiece before treatment, and (d) after treatment.

Figure 12 shows $250\times$ SEM micro images comparing the surface of the Inconel 625 bars after polishing by different types of abrasive particles. In order to compare the polishing characteristics of each abrasive particle (such as CNT with diamond paste (1st), Al_2O_3 (2nd), and SiC (3rd)), SEM micro images of the workpiece after polishing by each abrasive were used. It is observed that the surface quality of Inconel 625 bars was significantly improved by each abrasive particle, which the surface roughness of the workpiece was reduced from $0.31\ \mu\text{m}$ to $0.02\ \mu\text{m}$, $0.03\ \mu\text{m}$, and $0.06\ \mu\text{m}$ by CNT with diamond paste (1st), Al_2O_3 (2nd), and SiC (3rd). According to Figure 12, the surface conditions of the workpiece are different. The smoothest surface of the workpiece was obtained with CNT with diamond paste followed by Al_2O_3 , and SiC abrasive particles. In the case of CNT with diamond paste (1st), the surface of the workpiece is quite smooth and the original marks from the original surface were completely removed. In the case of Al_2O_3 , and SiC

abrasives, the surfaces of workpieces also look smooth but the multiple original marks from the original surface still remain.

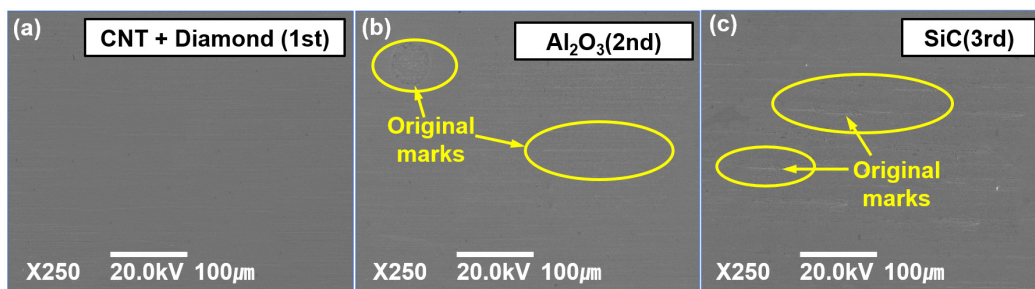


Figure 12. SEM micro images comparing the surface of the Inconel 625 bars after polishing by different types of abrasive particles: (a) CNT + diamond (1st), (b) Al_2O_3 (2nd), and (c) SiC (3rd) abrasives.

5.3. FEA Structural Analysis

To determine the material suitability of Inconel 625 as a solenoid valve STEM part for hydrogen tanks, 3D-modeled needle valves were designed according to the actual size of a needle valve, and their strain, equivalent stress, and safety factor were calculated using the Ansys structural analysis program. In this work, the Ansys Workbench Static Structural software 2022 R1 was used to conduct the FEA structural analysis of von Mises stress for two materials. The analysis was performed by applying a pressure of 700 bar to common STS 316 and novel Inconel 625 material under current hydrogen tank specifications. In all three analyses, the fixed conditions were given to the parts that had contact areas between the end of the solenoid valve stem (such as Inconel 625, and STS 316 bar) and the inner wall of the valve. Figure 13 shows the design of a solenoid valve of a hydrogen tank: (a) a full 3D model of a solenoid valve and (b) a schematic of a valve. Figure 14 shows the maximum total deformation and von Mises stress results for two materials. The analysis results are shown in Table 5. The two materials exhibited slightly varying maximum and average deformations—STS 316L showed values of 0.008183 (maximum) and 0.001085 (average), while Inconel 625 produced those of 0.009808 (maximum) and 0.001295 (average). Table 6 presents the results of a detailed von Mises stress analysis, indicating that both materials reached maximum stress at the solenoid end. However, Inconel 625 displayed a slightly higher stress of 0.06 MPa compared to STS 316L. The safety factors of the two materials were 4.6563 and 4.6539, respectively. The unique mechanical properties of these materials, despite identical structural pressure, lead to diverse stress patterns and distinct deformation behaviors. Notably, Inconel 625 boasts a high strength of up to 550 MPa, surpassing the 170 MPa of STS 316L. This difference in strength enables Inconel 625 to withstand high pressure, indicating it as an ideal material for a safety valve solenoid for STEM applications. Its superior mechanical properties and high surface quality effectively prevent fluid leakage and minimize friction with the contacting walls.

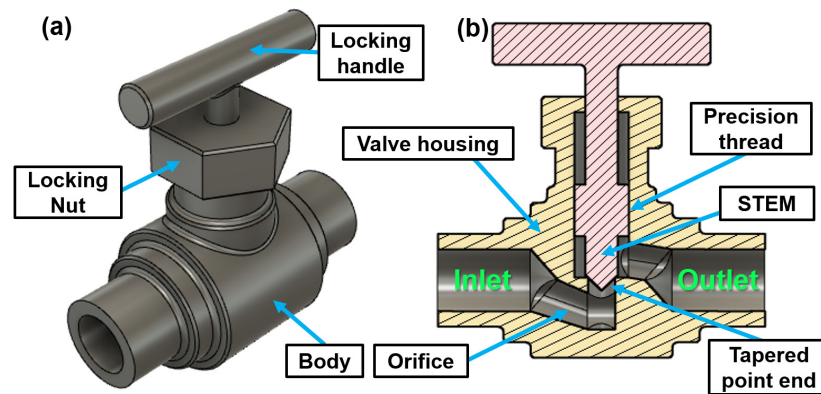


Figure 13. Design of a solenoid valve used for a hydrogen tank: (a) a full 3D model and (b) a schematic view of solenoid valves.

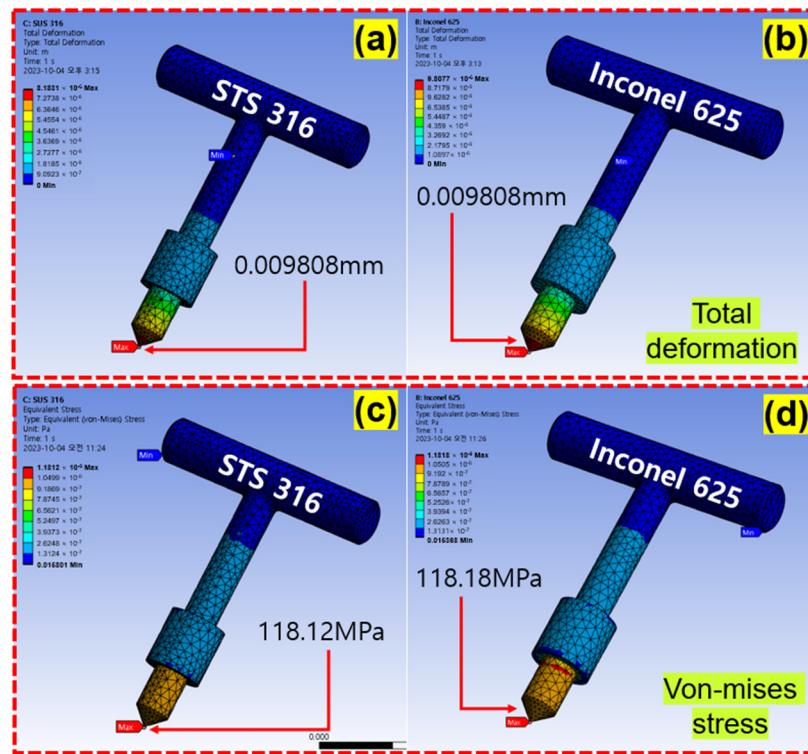


Figure 14. Maximum total deformation and von Mises stress results for two materials: (a) total deformation of STS 316, (b) total deformation of Inconel 625, (c) von Mises stress of STS 316, and (d) von Mises stress of Inconel 625.

Table 5. Total deformation analysis results.

Total Deformation (mm)	Maximum	Average
STS 316	0.008183	0.001085
Inconel 625	0.009808	0.001295

Table 6. Von Mises stress analysis results.

Von Mises Stress (MPa)	Maximum	Average	Safety Factor
STS 316	118.12	4.8463	4.6563
Inconel 625	118.18	4.8539	4.6539

6. Conclusions

The purpose of this study is to evaluate the suitability of Inconel 625 materials instead of STS 316 as a solenoid valve for hydrogen tanks in the hydrogen fuel cell market. To maintain confidentiality and prevent hydrogen embrittlement, the surface roughness of STEM was improved using super-fast MAF processing. The Ansys Workbench Static Structural software 2022 R1 was used to conduct the FEA structural analysis of von Mises stress for two materials such as (i.e., Inconel 625, and STS 316 bars).

1. A super-fast MAF process is suitable for reducing the surface roughness Ra values of Inconel 625 bars effectively. Based on the results, the Ra values of Inconel 625 bars were successfully reduced from 0.31 μm to 0.02 μm , 0.03 μm , and 0.06 μm by the CNT + diamond paste, Al_2O_3 , and SiC abrasives.
2. The best results of reduction in surface roughness were obtained under optimal conditions such as rotational speed of Inconel 625 bars: 15,000 RPM; abrasive particles: CNT + diamond paste; and processing time: 12 min.
3. According to the surface and SEM images of Inconel 625 bars before and after the super-fast MAF process, the rough parts (such as scratches and unevenness) were completely removed from the surface of Inconel 625 bars, and the surface condition after polishing was achieved to a super-smooth surface level (Ra: 0.02 μm).
4. FEA structural analysis results showed suitable strain (0.009808 mm), equivalent stress (118.18 MPa), and safety factor (4.6539) of the Inconel 625 bar, indicating that Inconel 625 is suitable for use as a valve material for hydrogen tanks.

Author Contributions: Conceptualization, H.-J.K.; methodology, H.-J.K.; writing—original draft H.-J.K.; supervision, project administration and writing—review and editing, L.H. and S.-D.M. All authors have read and agreed to the published version of the manuscript.

Funding: This research was supported by the National Research Foundation of Korea (NRF) (Research Project No. 2022R1F1A1073584) and the Basic Science Research Program through the National Research Foundation of Korea (NRF) funded by the Ministry of Education (No. RS-2023-00246193).

Data Availability Statement: The original contributions presented in the study are included in the article, further inquiries can be directed to the corresponding author.

Conflicts of Interest: The authors declare no conflicts of interest.

References

1. Song, Y.; Zhang, C.; Jia, Q.; Birgersson, E.; Han, M.; Zhang, P. Novel closed anode pressure-swing system for proton exchange membrane fuel cells. *Int. J. Hydrogen Energy* **2020**, *45*, 17727–17735. [[CrossRef](#)]
2. Das, L.M.; Gulati, R.; Gupta, P.K. A comparative evaluation of the performance characteristics of a spark ignition engine using hydrogen and compressed natural gas as alternative fuels. *Int. J. Hydrogen Energy* **2000**, *25*, 783–793. [[CrossRef](#)]
3. Matsuoka, S.; Yamabe, J.; Matsunaga, H. Criteria for determining hydrogen compatibility and the mechanisms for hydrogen-assisted, surface crack growth in austenitic stainless steels. *Eng. Fract. Mech.* **2016**, *153*, 103–127. [[CrossRef](#)]
4. Lee, H.J.; Ahn, J.; Kim, H.-Y. Design of a Solenoid Actuator for a Cylinder Valve in a Fuel Cell Vehicle. *Appl. Sci.* **2016**, *6*, 288. [[CrossRef](#)]
5. Ye, J.; Cui, J.; Hua, Z.; Xie, J.; Peng, W.; Wang, W. Study on the high-pressure hydrogen gas flow characteristics of the needle valve with different spool shapes. *Int. J. Hydrogen Energy* **2023**, *48*, 11370–11381. [[CrossRef](#)]
6. Kim, R.-W.; Hwang, K.-H.; Kim, S.-R.; Lee, J.-H. Investigation of Ultra-High Pressure Gas Control System for Hydrogen Vehicles. *Energies* **2020**, *13*, 2446. [[CrossRef](#)]
7. Ariyadi, H.M.; Jeong, J.; Saito, K. Computational analysis of hydrogen flow and aerodynamic noise emission in a solenoid valve during fast-charging to fuel cell automobiles. *J. Energy Storage* **2022**, *45*, 103661. [[CrossRef](#)]

8. Ye, J.; Zhao, Z.; Zheng, J.; Salem, S.; Yu, J.; Cui, J.; Jiao, X. Transient Flow Characteristic of High-Pressure Hydrogen Gas in Check Valve during the Opening Process. *Energies* **2020**, *13*, 4222. [[CrossRef](#)]
9. Takaki, S.; Nanba, S.; Imakawa, K.; Macadre, A.; Yamabe, J.; Matsunaga, H.; Matsuoka, S. Determination of hydrogen compatibility for solution-treated austenitic stainless steels based on a newly proposed nickel-equivalent equation. *Int. J. Hydrogen Energy* **2016**, *41*, 15095–15100. [[CrossRef](#)]
10. Liu, J.; Zhao, M.; Rong, L. Overview of hydrogen-resistant alloys for high-pressure hydrogen environment: On the hydrogen energy structural materials. *Clean Energy* **2023**, *7*, 99–115. [[CrossRef](#)]
11. Hicks, P.; Altstetter, C. Internal hydrogen effects on tensile properties of iron-and nickel-base superalloys. *Metall. Trans. A* **1990**, *21*, 365–372. [[CrossRef](#)]
12. Hicks, P.; Altstetter, C. Hydrogen-enhanced cracking of superalloys. *Metall. Trans. A* **1992**, *23*, 237–249. [[CrossRef](#)]
13. Cheung, C.F.; Wang, C.J.; Cao, Z.C.; Ho, L.T.; Liu, M.Y. Development of a multi-jet polishing process for inner surface finishing. *Precis. Eng.* **2018**, *52*, 112–121. [[CrossRef](#)]
14. Nagdeve, L.; Dhakar, K.; Kumar, H. Development of novel finishing tool into Magnetic Abrasive Finishing process of Aluminum 6061. *Mater. Manuf. Process.* **2020**, *35*, 1129–1134. [[CrossRef](#)]
15. Barman, A.; Das, M.J. Simulation and experimental investigation of finishing forces in magnetic field assisted finishing process. *Mater. Manuf. Process.* **2018**, *33*, 1223–1232. [[CrossRef](#)]
16. Heng, L.; Kim, Y.; Mun, S. Review of Superfinishing by the Magnetic Abrasive Finishing Process. *High Speed Mach.* **2017**, *3*, 42–55. [[CrossRef](#)]
17. Jiao, A.; Quan, H.; Li, Z.; Chen, Y. Study of magnetic abrasive finishing in seal ring groove surface operations. *Int. J. Adv. Manuf. Technol.* **2016**, *85*, 1195–1205. [[CrossRef](#)]
18. Xu, J.; Zou, Y.J. Development of a new magnetic abrasive finishing process with renewable abrasive particles using the circulatory system. *Precis. Eng.* **2021**, *72*, 417–425. [[CrossRef](#)]
19. Singh, M.; Singh, A.K. Magnetorheological finishing of variable diametric external surface of the tapered cylindrical workpieces for functionality improvement. *J. Manuf. Process.* **2021**, *61*, 153–172. [[CrossRef](#)]
20. Singh, M.; Singh, A.K. Magnetorheological finishing of copper cylindrical roller for its improved performance in printing machine. *Proc. Inst. Mech. Eng. Part E J. Process Mech. Eng.* **2021**, *235*, 103–115. [[CrossRef](#)]
21. Rana, A.S.; Bedi, T.S.; Grover, V. Fine-finishing of stepped cylindrical workpiece using magnetorheological finishing process. *Mater. Today Proc.* **2021**, *41*, 886–892. [[CrossRef](#)]
22. Nguyen, D.N.; Chau, N.L.; Dao, T.-P.; Prakash, C.; Singh, S. Experimental study on polishing process of cylindrical roller bearings. *Meas. Control* **2019**, *52*, 1272–1281. [[CrossRef](#)]
23. Choudhury, I.A.; El-Baradie, M.A. Machinability of nickel-base super alloys: A general review. *J. Mater. Process. Technol.* **1998**, *77*, 278–284. [[CrossRef](#)]
24. Buddaraju, K.M.; Sastry, G.R.K.; Kosaraju, S. A review on turning of Inconel alloys. *Mater. Today Proc.* **2021**, *44*, 2645–2652. [[CrossRef](#)]
25. Blakey-Milner, B.; Gradl, P.; Snedden, G.; Brooks, M.; Pitot, J.; Lopez, E.; Leary, M.; Berto, F.; du Plessis, A. Metal additive manufacturing in aerospace: A review. *Mater. Des.* **2021**, *209*, 110008. [[CrossRef](#)]
26. Parida, A.K.; Maity, K. Comparison the machinability of Inconel 718, Inconel 625 and Monel 400 in hot turning operation. *Eng. Sci. Technol. Int. J.* **2018**, *21*, 364–370. [[CrossRef](#)]
27. Yun, H.; Han, B.; Chen, Y.; Liao, M. Internal finishing process of alumina ceramic tubes by ultrasonic-assisted magnetic abrasive finishing. *Int. J. Adv. Manuf. Technol.* **2016**, *85*, 727–734. [[CrossRef](#)]
28. Singh, G.; Kumar, H.; Kansal, H.K.; Srivastava, A.J. Effects of chemically assisted magnetic abrasive finishing process parameters on material removal of Inconel 625 tubes. *Procedia Manuf.* **2020**, *48*, 466–473. [[CrossRef](#)]
29. Liu, J.; Zou, Y. Study on Elucidation of the Roundness Improvement Mechanism of the Internal Magnetic Abrasive Finishing Process Using a Magnetic Machining Tool. *J. Manuf. Mater. Process.* **2023**, *7*, 49. [[CrossRef](#)]
30. Xie, H.; Zou, Y.; Dong, C.; Wu, J. Study on the magnetic abrasive finishing process using alternating magnetic field: Investigation of mechanism and applied to aluminum alloy plate. *Int. J. Adv. Manuf. Technol.* **2019**, *102*, 1509–1520. [[CrossRef](#)]
31. Kausar, A.; Ilyas, H.; Siddiq, M. Current Research Status and Application of Polymer/Carbon Nanofiller Buckypaper: A Review. *Polym. Plast. Technol. Eng.* **2017**, *56*, 1780–1800. [[CrossRef](#)]
32. Heng, L.; Yang, G.E.; Wang, R.; Kim, M.S.; Mun, S.D. Effect of carbon nano tube (CNT) particles in magnetic abrasive finishing of Mg alloy bars. *J. Mech. Sci. Technol.* **2015**, *29*, 5325–5333. [[CrossRef](#)]
33. Abubakr, M.; Hegab, H.; Osman, T.A.; Elharouni, F.; Kishawy, H.A.; Esawi, A.M.K. Carbon Nanotube-Based Nanofluids. In *Handbook of Carbon Nanotubes*; Abraham, J., Thomas, S., Kalarikkal, N., Eds.; Springer International Publishing: Cham, Switzerland, 2022; pp. 1501–1532. [[CrossRef](#)]
34. Postek, E.; Sadowski, T. Impact model of the Al₂O₃/ZrO₂ composite by peridynamics. *Compos. Struct.* **2021**, *271*, 114071. [[CrossRef](#)]

Disclaimer/Publisher’s Note: The statements, opinions and data contained in all publications are solely those of the individual author(s) and contributor(s) and not of MDPI and/or the editor(s). MDPI and/or the editor(s) disclaim responsibility for any injury to people or property resulting from any ideas, methods, instructions or products referred to in the content.